Proceedings of ASME Turbo Expo 2022
Turbomachinery Technical Conference and Exposition
GT2022
June 13-17, 2022, Rotterdam, The Netherlands

GT2022-82130

MULTI OPERATING POINT AERODYNAMIC OPTIMIZATION OF A RADIAL COMPRESSOR IMPELLER FOR AN APPLICATION IN HIGH TEMPERATURE HEAT PUMP

Robert Schaffrath*, **Maximilian Kriese, Bojan Kajasa, Martino Köhler, Eberhard Nicke**
Department of High Temperature Heat Pump
Institute of Low-Carbon Industrial Processes
German Aerospace Center
Zittau, 02763
Email: robert.schaffrath@dlr.de

Christian Voß
Department of Fans and Compressors
Institute of Propulsion Technology
German Aerspace Center
Cologne, 51147
Email:christian.voss@dlr.de

ABSTRACT

The decarbonization of production processes plays an important role on the way to environmentally friendly economy. Especially, the implementation of high temperature heat pumps (HTHP) offers a great potential to replace fossil fuel-based energy infrastructure. A major issue for the introduction of HTHP is the initial cost and regarding the payback period. However, there is still potential in increasing the coefficient of performance (COP) of HTHP for the economic integration in existing industrial processes. One important possibility is the dedicated development and design of turbocompressors for this application and the planned heat transfer medium including the aerodynamic optimization of compressor geometry. Against this background an automated aerodynamic optimization method for radial compressor blade geometry for superheated steam is presented. The optimization refers to two different operating points of the HTHP and focuses on maximizing the isentropic efficiency of the impeller geometry as well as the pressure ratio. The algorithm is accelerated by data-driven metamodels and is implemented in a high-performance cluster environment. The boundary condition of the inherent computational fluid dynamics (CFD) calculation comes from the thermodynamic cycle calculation of the whole HTHP system. A two-stage compression with intercooling between the compressor stages are foreseen. Our approach shows an increment of both objective functions in both operating points and the satisfaction of further side conditions for the low pressure compressor (LPC). Furthermore, it results in an increment of 5 percent points of isentropic efficiency and 13 percent points of static to total pressure ratio in comparison to our initial geometry. These impeller optimizations result in a COP increment of 5 percent. The resulting geometry will be interpreted in the context of aerodynamic behavior. Based on that results additionally, a flow-cut optimization for the high pressure compressor (HPC) is given and evaluated. The results are comparable to aerodynamic optimization in different research fields like aircraft engines or stationary gas turbines and contribute to optimized multistage compressor design for HTHP.

NOMENCLATURE

HTHP	High temperature heat pump
COP	Coefficient of performance
CFD	Computational fluid dynamics
LPC	Low pressure compressor
HPC	High pressure compressor
$\dot{Q}_{Sink}$	Heat flow to heat sink
$\dot{W}_{total}$	Total input work to high temperature heat pump
η_{Engine}	Efficiency of engine
$\eta_{Gearbox}$	Efficiency of gearbox

*Address all correspondence to this author.

$\eta_{is,comp}$ Isentropic efficiency of compressor
$\eta_{electric}$ Efficiencies of all electric device
UDP User defined process chain
RPM Rotations per minute
RANS Reynolds-Averaged Navier-Stokes equation
$\pi_{ts}^{Op_*}$ Total to static pressure ratio for operation point $*$
η^{Op_*} Isentropic efficiency for operation point $*$
$\dot{m}^{Op_*}$ Mass flow $\frac{kg}{s}$ for operation point $*$
LE Leading edge of compressor impeller
TE Trailing edge of compressor impeller
FE Finite element

INTRODUCTION

Motivation

The industrial sectors are responsible for approximately 25% of all green house gas emissions. Most of the used energy is required for process heat supply [1]. Most of the process heat is produced by combustion of fossil fuel (i.e. coal or gas). The required heat can be divided in three temperature classes: <100 °C, 100-500 °C and >500 °C. Especially for process heat below 500 °C there are fossil fuel free alternatives in research and development. A promising research topic are High Temperature Heat Pumps (HTHP) with a heat sink above 150 °C. Key components of HTHP are compressors, heat exchanger and used refrigerants. The optimal combination of components delivers a high Coefficient of Performance (CoP) which is defined as the ratio of thermal energy output to electrical energy input. A high value of CoP is essential for a fast return of invest by integration of a HTHP in an existing industrial process. The scope of this paper is the description of an optimization process for both the raise of pressure ratio and isentropic efficiency.

Literature review

The penetration of HTHP as an ecological and economical alternative to the provision of industrial process heat depends according to Arpagaus ([2] and [3]) on three essential criteria:

- closing the knowledge gaps or reducing prejudices
- the use of environmentally friendly refrigerants (working medium)
- the development of mass-produced components.

For many reasons, water or steam is a very suitable working medium for HTHP. Compared to other refrigerants - such as those used in heat pumps - water is environmentally friendly, harmless, inexpensive. Morover the latant heat is for example 15 times higher than R134, which offers especially in high sink temperature a great potential ([4] and [5]). In HTHP, one of the most important components is the compressor unit. This is usually designed as a screw or piston compressor. In contrast, turbo machines are rarely used in commercially available heat pumps (including HTHP) [3]. In general, due to their compact design, high stage pressure ratios and good efficiency, centrifugal compressors in particular can cover a wide range of applications in the future [6]. Nowadays, powerful computers have significantly reduced the simulation times of 3D flows, but the preliminary design of centrifugal compressors (in this context impeller, diffuser) is and remains an important design step. These preliminary design procedures are based on empirical values and model assumptions (see for example [7]). Because of that, in certain operating areas e.g. the occurrence of choke and surge the ability for the predication of the behavior of the turbomachinery is limited. For example, Meroni et al. [6] have shown that their preliminary design tool is capable to predict the behavior of the turbomachinery for various refrigerants. Nevertheless, in comparison to their CFD and experimental results there is a certain deviation. A first impeller geometry was derived based on a known design. Automated aerodynamic optimization is a common practice in engineering of turbo compressors. Kim presented in [8] a multi objective optimization approach with evolutionary algorithms for a centrifugal compressor. Objectives were isentropic efficiency and total to total pressure ratio. The evolutional approach is accelerated by surrogate models. The optimization resulted in an increment of approx. 0.5% of efficiency and 1% of pressure ratio. Another aerodynamic optimization for increasing isentropic efficiency and operating range was done by Raitor in [9]. It was realized by CFD calculations of the operating points inside an automatic process chain. One of the pareto-optimal members increased the impeller peak efficiency by 1.9 percent nevertheless the operating range could not be expanded. Another aerodynamic optimization approach with one dimensional calculations is given by Li in [10]. It was figured out that the one dimensional approach is basically the same than a 3D CFD calculation, which shows that the used program is reliable and effective. A transonic centrifugal compressor impeller geometry was optimized by Hehn [11]. For the initial geometry, the SRV4 impeller was used. The objective was to increase the isentropic efficiency as well as the acoustic behaviour of the compressor. It was done by the weighted sum of 8 objective functions. Three operating points were considered. The process was started with 231 samples in a database and resulted in a solution set of 672 converged members. In summary the isentropic total-to-static efficiency could be increased by 1.4 % points. An alternative approach for the optimization of the surge margin of centrifugal compressors was presented by Ratz [12]. They were defining a new objective function through the summation of throat to peak mach number ratios at different blade spans for impeller and vaned diffusor geometry. A benchmark with a conventional objective function for surge margin showed nearly the same results. The results of a structurally constraint aerodynamic optimization for an axial compressor was shown in 2021 by Cuciumita [13]. Based on the initial geometry of the NASA rotor 37, a free form deformation for blade generation and the efficiency as objective function,

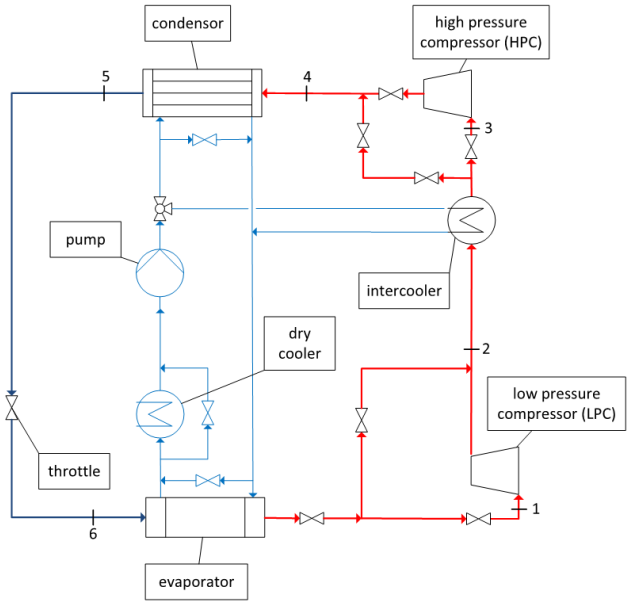

FIGURE 1. Schematic representation of the HTHP

a von Mises stress constrained calculation is carried out. The stress constraint was realized by a pre-calculated response surface function and evaluated during the optimization process. It was possible to achieve an efficiency increment of 3% with satisfied stress constraint. Furthermore, it was presented that an unconstrained optimization resulted in an efficiency increment of 4%.

RESEARCH SETTING AND METHODS

Cycle simulation of HTHP system

This paper describes the development of a compressor that is part of an HTHP based on the counter-clockwise Rankine cycle. The compressors suck in superheated steam and compress it to a defined final pressure (see 2 and 4 in Figure 1). The water vapor (see 5 in Figure 1) is then condensed and expanded to the initial pressure level (see 6 in Figure 1). The water evaporates again in the evaporator and the initial state (see 1 in Figure 1) is reached. The thermodynamic design of the cycle is done with the FlowChart software Ebsilon [14]. The design of the cycle is based on the one hand on the fact that a defined condensation temperature (point 5 in Figure 1) is to be achieved. On the other hand, there is no vacuum technology, which means that the boundary conditions in points 1 and 6 are specified. As a result, the overall pressure ratio is defined and a two-stage design was chosen.

$$COP = \frac{\sum \dot{Q}_{Sink}}{\frac{\dot{W}_{total}}{\eta_{Engine}\eta_{Gearbox}\eta_{is,comp}\eta_{electric}}} \tag{1}$$

In earlier studies (see Lachner [15]) it was found that the cycle process achieves the greatest possible efficiency (max. COP), see equation 1 and Zühlsdorf ([16]), when every compressor has to achieve the same pressure ratio. The target mass flow is the result of a specified shaft power. This defines the thermodynamic entry conditions of the respective compressor stages. In addition to the design point, an off-design calculation was carried out for another operating point, which must be considered as a further restriction in the aerodynamic optimization.

Optimization approach

For the optimization of the impeller geometry of LPC the DLR optimization package *AutoOpti* is used. *AutoOpti* implements a surrogate model accelerated evolutionary optimization strategy for user defined objectives. The objectives will be defined by a user defined process chain (UDP). Within the UDP individualized batch jobs can be defined for given optimization parameters. The return of the UDP is a vector of simulation results like aerodynamical or structural values (hereinafter referred to as flow parameters) that can be used for the fitness function definition. The used surrogate model implements a Kriging strategy (see i.e. [17]) for the estimation of flow parameter calculated with previous computed UDPs. Furthermore, *AutoOpti* allows the integration of constraints for the optimization problem definition by implementing an additional penalty term. Moreover, it is possible to solve multi objective problems without super position of single objective functions (see [18], [19] and [20]).

Process chain for LPC

A detailed explanation of our implemented UDP will be given in this section and Figure 2 visualizes the different steps. The first process is the design of the hub and tip line of the radial compressor, which defines the flow path of the impeller blade. Realized by a splined interpolation of the initial flow path, 6 parameters which control the location of supporting points are defined. Each of these points can only move either in axial direction (**X**), radial direction (**R**) or normal to hub line, respectively tip line. It is shown in Figure 3 that the first control parameter (OPTIPARAM_Strak_1) shifts the first 10 points of the tip line in radial direction, the next three parameters OPTIPARAM_Strak_1 to OPTIPARAM_Strak_3 modifying the next three supporting points normal to the tip line and the fifth parameters (OPTIPARAM_Strak_5) moves the outlet point in axial direction. The hub line is only controlled via one supporting point in normal direction (OPTIPARAM_Strak_6).

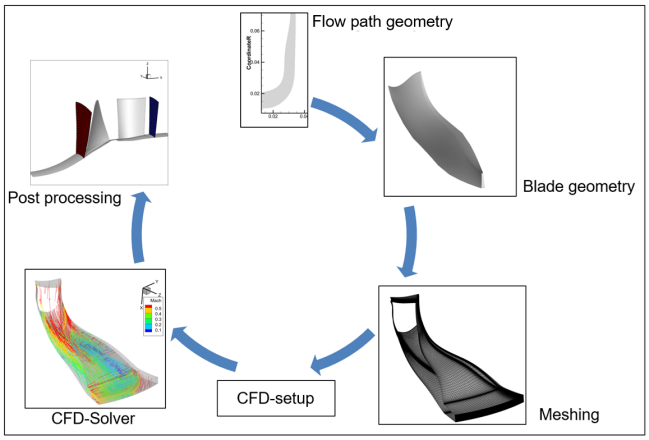

FIGURE 2. UDP for optimisation process of LPC

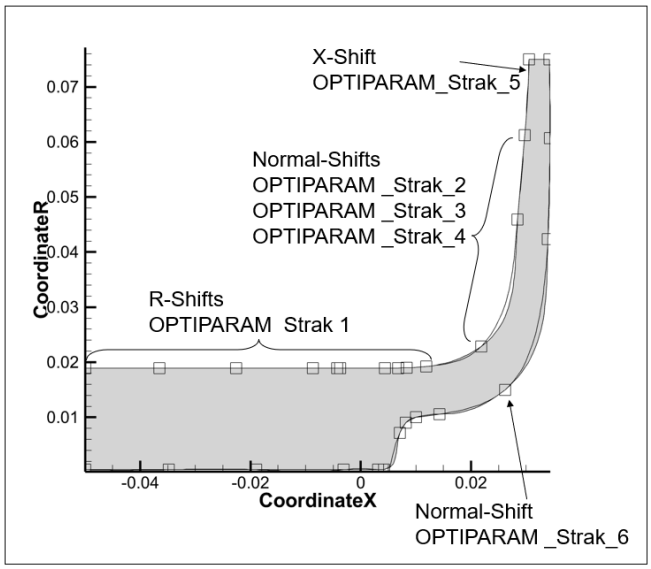

FIGURE 3. Flow path supporting points and shift parameters

The next step is the creating of the blade geometry. The creation of axial and radial compressor blades is done with the DLR intern tool *BladeGenerator* (see [21]). *BladeGenerator* calculates the blade appearance by the interpolation of profile lines starting from hub to tip line. Each of these profiles can be individually modified regarding angle of attack, angle of inflow, angle of outflow, thickness distributions, rake angle, interpolation points (defined by DeBoor-points), radi of leading and trailing edge. The construction profiles used for our blade design are shown in Figure 4. Furthermore, the diameter of the impeller is fixed to 130 mm. Nevertheless, the starting point of the leading edge is a free variable to the optimizer as well as the number of

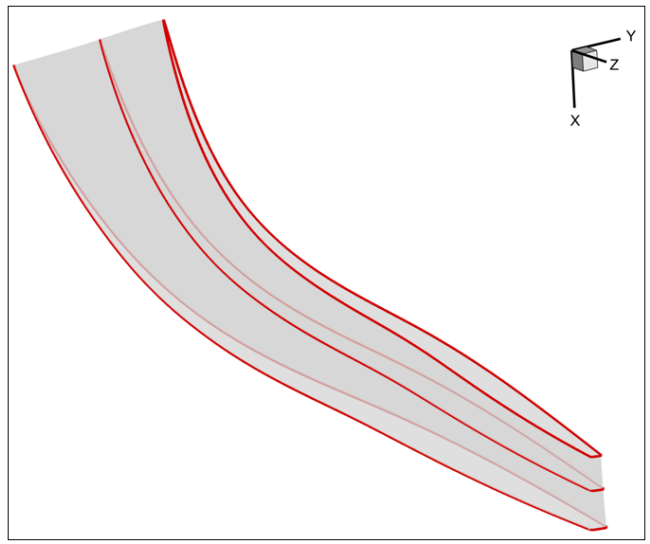

FIGURE 4. Construction profiles for initial blade design

used blades. The rotations per minute (RPM) as well as the back pressure for the CFD which defines the operating point are free variables and can be set during the optimization process.

The meshing process of the CFD domain continues our UDP. For that part an DLR in-house structured multiblock grid generator is used, which generates a structured mesh based on O-C-H topology containing 1.45 million cells (see [22]). Meshing of the blunt trailing edge is considered. A meshing of the fillet on the hub side of the impeller blade is not applied. The tip clearance region on the impeller blade is realized with a structured block. The CFD Mesh of the impeller can be seen in Figure 5. Cause of impeller periodicity only one blade passage of the full anulus is calculated. This decreases the simulation time immensely.

Based on the created mesh the CFD setup is generated. For the calculation of the flow field, the Reynolds-Averaged Navier-Stokes Equation (RANS) are solved (steady state). The ideal gas model and the Sutherland law for viscosity model is also used for the simulation. In general, the usage of the law of ideal gas and its fundamental equations are limited to a certain application area (see [23]). The difference of the properties of superheated steam calculated by the ideal gas equation compared to those based on the established steam tables is expressed by the compressibility factor Z. That means, for an compressibility factor of 1 the gas can be seen as ideal, which is especially valid for a state of superheated steam properties in regions of very low pressure and very high temperatures. The compressibility factor varies in between 0.97 and 0.995 in the presented simulation. Therefore, a maximum error of three percent for the superheated steam occurs while using the law of ideal gas instead of the steam table. In addition to that, we have run simulation, which are not part of the

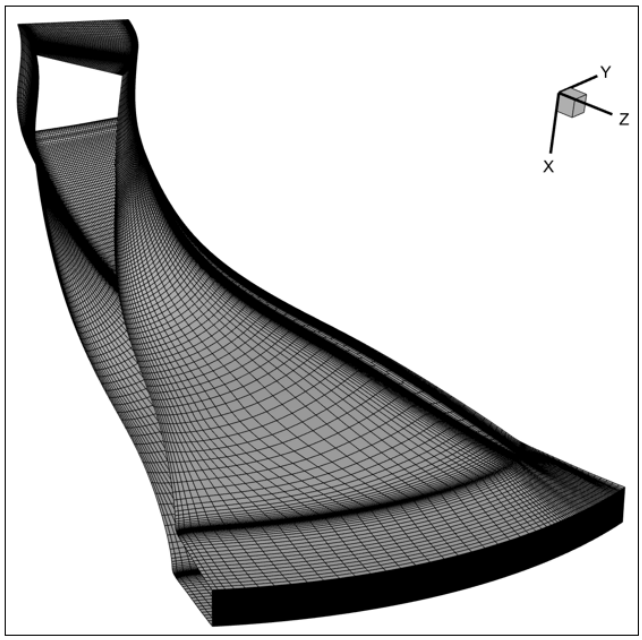

FIGURE 5. CFD mesh

present work, with different steam properties (specific gas constant, isentropic exponent, viscosity etc.). In these simulations the general boundary conditions such as the massflow and the inlet pressure were kept constant. Afterwards the simulations are evaluated regarding total-to-total pressure ratio and efficiency. It was figured out that the differences could be neglected as well. Because of that, we considered the treatment of steam as ideal gas is sufficient especially regarding the time savings for simulation.

The discretization is realized with a second order finite volume scheme. The mesh has a sufficient resolution for a low Reynolds boundary condition, thus no wall functions are necessary. For the turbulence model, Menter SST is selected. Furthermore, the solver is back pressure controlled and for convergence the variation of massflow, isentropic efficiency and pressure ratio has to be below 0.01% for 200 time steps. The optimization is done on a cluster computer and for an efficient calculation the CFD domain is separated to 64 cores. For the CFD setup preprocessing a script based in-house tool is used. After successful setup generation, the flow simulation is done with the DLR intern tool TRACE (Turbomachinery Research Aerodynamic Computational Environment, see [24]).

Multi operating point optimization

$$\begin{aligned} &\max \pi_{ts}^{Op_1} + \pi_{ts}^{Op_2} \\ &\max \eta^{Op_1} + \eta^{Op_2} \end{aligned} \tag{2}$$

$$\begin{aligned} \dot{m}^{Op_1} &\geq 0.216 \\ \dot{m}^{Op_2} &\geq 0.223 \\ \pi_{ts}^{Op_1} &\geq 1.6 \\ \pi_{ts}^{Op_2} &\geq 1.6 \\ \eta^{Op_1} &\geq 0.85 \\ \eta^{Op_2} &\geq 0.85 \end{aligned} \tag{3}$$

There are six constraints and two objectives which have to taken into account for the multi operating point aerodynamic optimization problem. The ratio of static pressure at the evaluation section to the total pressure of the inlet plane is used below with $\pi_{ts}^{Op_*}, * \in \{1,2\}$. The isentropic efficiency is η^{Op_*} and the mass flow denoted with $\dot{m}^{Op_*}$. The target of our problem definition is the equally weighted optimization of both operation points regarding the isentropic efficiency and the total to static pressure ratio (see (2)). The reason for the choice of total to static compared in place of total to total pressure ratio is the reduction of losses in the volute. In the spiral, only a portion of the dynamic pressure is converted into static pressure, but the static pressure reached at the impeller outlet is already a plant-relevant result. The resulting mass flow is constrained to 0.216 $\frac{kg}{s}$ for the first and to 0.223 $\frac{kg}{s}$ for the second operating point. Also there are two more constraints for pressure ratio as well as efficiency to equalize the optimization behavior for both operating points (see (3)).

In Table 1 the limits of the physical design parameters are shown. It is noted that the parameters *LE Radius*, *TE Radius* and *Thickness* are correlated to an unstaggered normalized coordinate system so no units are written. There are more free variables which can be modified during the optimization process but they are pure numerically nature, like leading edge and rake contour supporting points and DeBoor points inside the flow path.

The optimization is started with pure mutation process unless a fixed number of converged UDP are available. There has to be at least 20 converged member for the optimization. After a successful initialization, the optimizer randomly decides whether new members will be generated by genetic strategies or by evaluations of the kriging surrogate models. The optimization is computed on a high performance computer environment maintained by DLR. The environment is divided into compute nodes with

TABLE 1. Boundaries of free variables

Name	LB	Initial value	UB
Stagger angle	55°	65°	105°
LE angle	40°	70°	110°
TE angle	40°	70°	90°
LE Radius	0.004	0.006	0.01
TE Radius	0.0017	0.005	0.01
Thickness	0.0124	0.045	0.05
#Blades	9	17	21
RPM^{OP_1}	78000 min^{-1}	78500 min^{-1}	85000 min^{-1}
RPM^{OP_2}	78000 min^{-1}	78500 min^{-1}	85000 min^{-1}
$\pi_{ts}^{Op_1}$	$1,5$	$1,9$	$2,25$
$\pi_{ts}^{Op_2}$	$1,7$	$1,7$	$2,3$

64 cores each. For the *AutoOpti* calculation, 15 compute nodes were allocated. The first node was running the master process which evaluates the surrogate models, store result data and generate new members. The second node was permanently updating the surrogate models based on the database of finished UDPs. Due to the huge database of calculated members, the updating of the surrogate models is very time consuming. The other 13 compute nodes computed parallel the UDP which comes from the master node.

Flow cut strategy for compressor HPC

Based on the results of optimization for LPC the flow cut for HPC will be calculated. The target of the flow cut is to shift the compressor map of a fix blade geometry by cutting the blade between hub and tip line. Nevertheless, this cut is neither parallel to hub nor tip line, so this problem is formulated as second optimization problem. The objective functions are kept equal (see (4)) but the constraints were changed to shift the operating range to the process requirements of the HPC (see (5)). The set of free variables is reduced to the interpolation of casing line, as well as the operating point specific RPMs and the back pressures. That results in 9 free variables for the flow cut optimization. The UDP will be kept the same. The algorithm will be initialized by a good member of the pareto front of optimization of LPC. The advantage of this approach is a similar structure mechanics as well as rotor dynamic behavior for HPC then for LPC.

$$\begin{aligned} &\max \pi_{ts}^{Op_1} + \pi_{ts}^{Op_2} \\ &\max \eta^{Op_1} + \eta^{Op_2} \end{aligned} \tag{4}$$

$$\begin{aligned} 0.2 \geq \dot{m}^{Op_1} \geq 0.23 \\ 0.21 \geq \dot{m}^{Op_2} \geq 0.24 \end{aligned} \tag{5}$$

RESULTS

Multi operating point optimization

The calculation time of the optimization was 5 days and started 7552 UDPs. The number of UDPs, which were successful and satisfied all constraints, is 3073. In Figure 6 the values of the objective functions of the converged and constraint satisfied members are shown. The abscissa correlates with the sum of isentropic efficiencies and the ordinate with the sum of pressure ratios. The pareto optimal members are visualized with red crosses in contrast to blue circles which belongs to non-pareto optimal members. Furthermore, the pareto front after 1000 successful members is shown in magenta and after 2000 in orange. It can be seen that geometries are calculated which have a combined efficiency of above 1.78 which means that the efficiency in both operating points is slightly under 90%. Furthermore, there are geometry calculations which have lower efficiencies but have high static to total pressure ratios in both operating points. The pareto front consists of 51 members.

The objectives of the initial geometry are a 3.6 as pressure ratio and 1.69 as efficiency for both operating points. Nevertheless, in Figure 6 the initial geometry is not shown because it does not satisfy the massflow constraints. For a better aerodynamic understanding, a member of the middle of the pareto front is selected to show the optimized geometry. In Figure 7 the flow path of member 7516 is shown. It can be seen that the flow path height at the leading edge is increased by 73% and at the trailing edge by 33%. The number of blades is 17, but the RPM in both operating points increased to 85.000, which is the upper limit. The back pressure in operating point one is increased to 399.343 Pa and 175.932 Pa for operation point two. The resulting geometry is shown in Figure 8.

Figure 9 show the flow path of the Impeller of the Initial geometry (left picture), member 0480 - a early stage of the optimization (in the middle) and of member 7516 (right side). The color map is linked with the static pressure after circumferential averaging of the 3 D-flow field. In contrast, the next figure (Figure 10) shows the corresponding velocity vectors in the S2M plane. The comparison between the starting geometry and the optimization results clearly shows the effect of the objective function on the impeller design especially for the blade hight. Not only the width

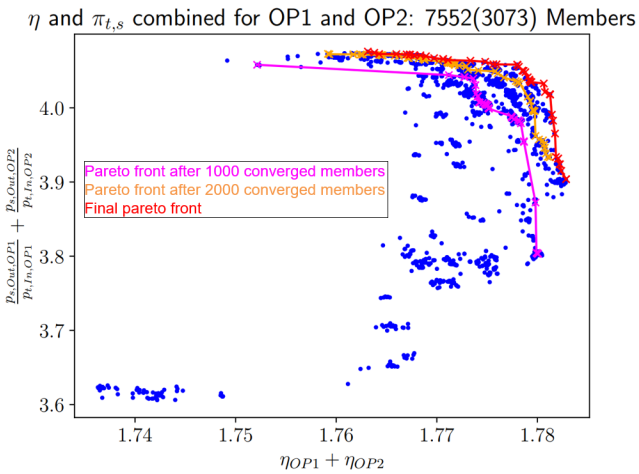

FIGURE 6. Converged members of optimization of LPC

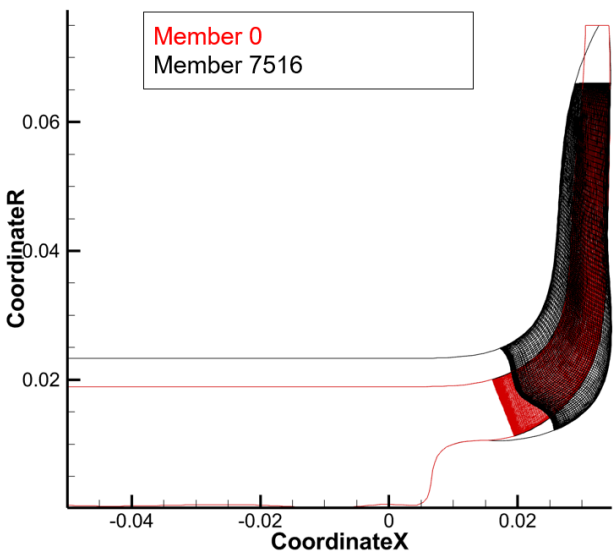

FIGURE 7. Initial and optimized flow path geometry

of the impeller outlet was increased to realize the mass flow rate at high static pressure, but also already at the impeller inlet. The velocity level in the area where the casing has the highest curvature could drastically reduce. In this area of the flow channel often flow separation or high flow losses could occur. The middle and right picture do not show serious differences here, but the losses could be further reduced and the efficiency increased.

Computational structure mechanics

Based on the final result of aerodynamic optimization, a baseplate was added under the final geometry of the blade. A

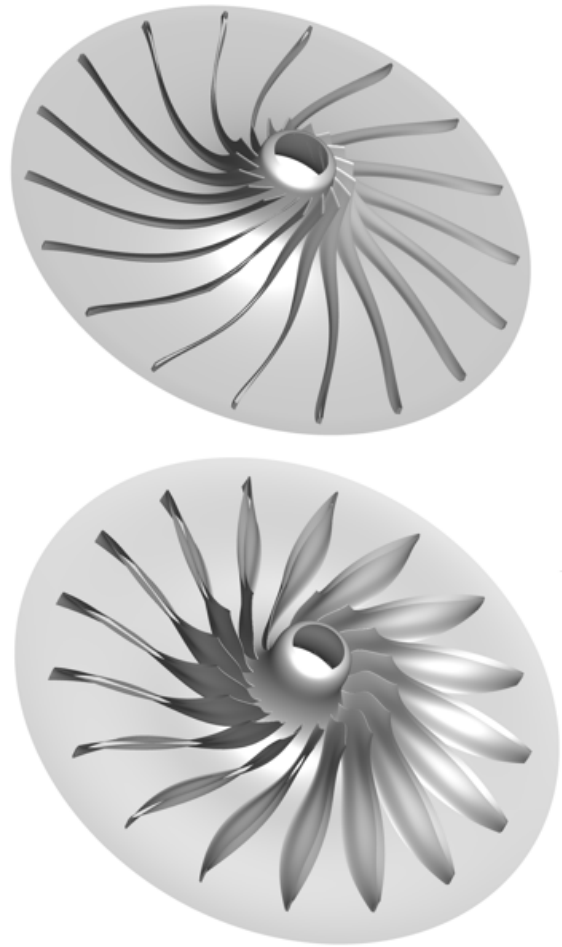

FIGURE 8. Initial and optimized impeller geometry

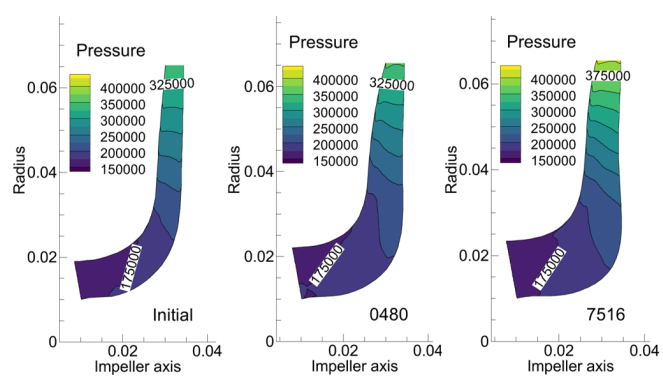

FIGURE 9. Static pressure of initial and optimized members

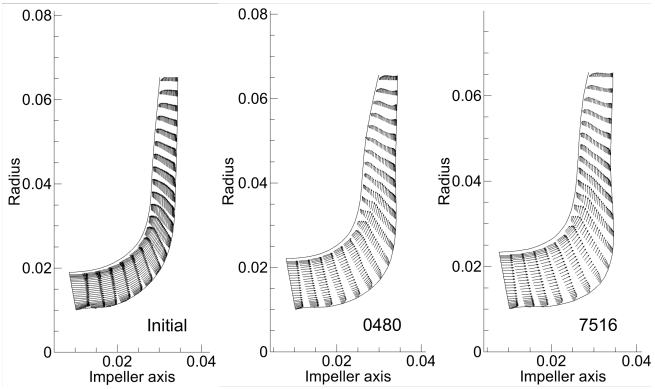

FIGURE 10. Velocity vectors of initial and optimized members

rotationally symmetrical component was created. The geometry of the front side is given by the blade, while the geometry of the back side is variable. The first geometries of backsides were based on experience. An FE model was then built up, which is characterized by its rotationally symmetrical support and to which the following loads were attached: Gravitational acceleration, rotation speed, pressure load from CFD on the front of the impeller and 80% of the maximum pressure as surface load on the back of the impeller. The von Mises equivalent stresses as well as the total deformations were calculated. The equivalent stresses were used to evaluate the strength, while the total deformations were used for a hot to cold transformation.

Flow cut for HPC

Based on member 7516 the Flow cut for HPC is calculated. The calculation time was 3 days and 1469 UDPs were started. 937 members converged and satisfied all constraints. These are shown in Figure 11. The abscissa and the ordinate are the same then in Figure 6 as well as the format of the pareto front. It can be seen that the upper limits of the efficiency and the pressure ratio of the pareto front of the HPC is lower than the limits of the pareto front of the LPC. In case of the efficiency there is a decrement of 5 percent points per operating point and for the pressure ratio 5% in summation. In Figure 12 the flow path of member 756 which is located in the middle of the pareto front is show in green. In black is the flow path of member 7516 which is the initial member and one of the results of the LPC optimization. The averaged flow path height decrement is nearly 25%.

Results of aerodynamic optimization in cycle simulation

The influence of the optimized aerodynamics on the performance of the HTHP (see Figure 1) was evaluated. This evaluation is carried out by qualitatively comparing the efficiency of the initial geometry with that of the optimized geometry. It was

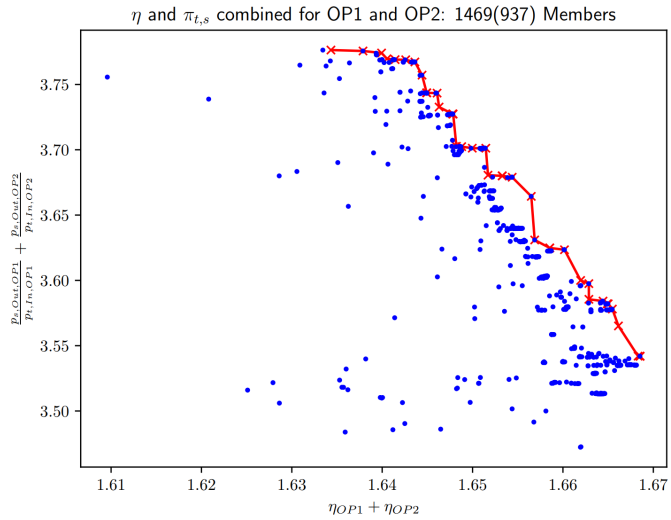

FIGURE 11. Converged members of FlowCut for HPC

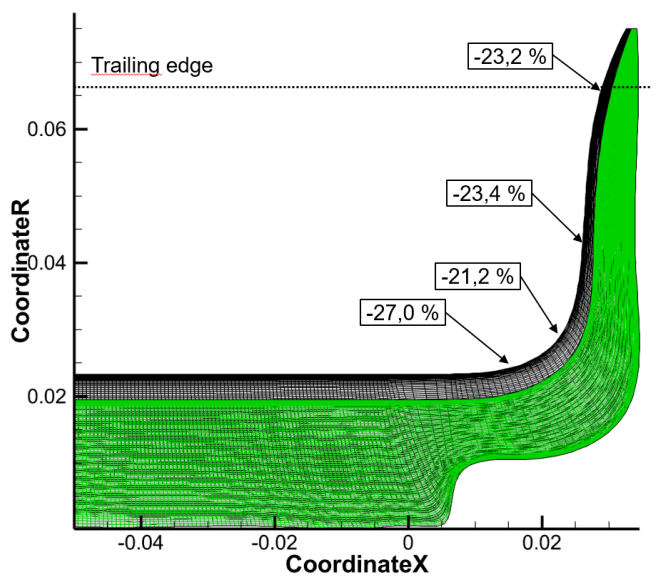

FIGURE 12. Comparison of flow path of LPC and HPC

assumed that the efficiency of the electric motors, the gearbox and the electrical losses are constant. The results only represent the improvement of the impeller. Therefore, based on numerical results, an estimation for the diffuser and volute losses was made. Those were kept constant for both the initial and the optimized geometry.

The isentropic impeller efficiency of the initial geometry is 83.5 percent. The increase in isentropic efficiency to 91 and 90.5 percent of the low-pressure and the high-pressure stage meant that

the COP of the system could be increased by 8.7 percent in the first and 8.9% in the second operating point. In general, if an improvement in the isentropic compressor efficiency of one percent is achieved, the COP of the HTHP increases by 1.05 percent.

DISCUSSION

The result for the aerodynamic LPC optimization is comparable to calculations that are found in the literature. Even with different boundary conditions (e.g. superheated steam), efficiencies which are close to 90 % have been achieved. That leads to an increment of approximately 5 percent points compared to our initial geometry. Furthermore, the pressure ratio could be improved by 13 percent points.

Unfortunately the use of the flow cut strategy could not generate results for the HPC that are comparable to the optimized LPC geometry in terms of efficiency and pressure ratio. Because of that, an HPC specific optimization will be investigated in the future.

OUTLOOK

Optimized vaned diffusor geometry

For further investigation, a vaned diffuser will be integrated in the optimization process of the impeller. The advantage of such a vaned diffuser is the conversion of the kinetic energy in the impeller rake into potential energy for the increase of the static pressure. The flow with the reduced velocity entering the volute has an influence on the loss occurring in it. Compared to the pressure loss in the vaned diffuser, the pressure loss in the volute is much smaller than without the vaned diffuser. For the optimization of the impeller with vaned diffuser, the flowpath is extended. In addition, parameters are included on the tip side geometry that can optimize the flowpath of the vaned diffuser. The angle of attack, the inlet and outlet flow angles, the thickness distribution as well as the number of blades are also released for the optimization process. First results have shown an increase of the static pressure of approximately 20-25% compared to the calculations of the vaneless diffuser.

Stress constrained optimization

The aerodynamic optimization tends towards thin blade thickness at the leading edge. This circumstance results in a large possible number of blades and minimizes the flow resistance. From a structural mechanics point of view, thin geometries have the potential for significant stress areas, which has been confirmed by calculations. Furthermore, a steep rise of the hub geometry leads to high stress values as well.

So, it was found out that the pure recalculation of an aerodynamically optimized geometry leads to a conflict between aerodynamics and structural mechanics. The problem areas identified in the structural mechanical calculation, as well as their elimination, often collide with the aerodynamic optimization.

Currently, improvements of the entire design process are under investigation. The structural mechanics should be integrated into the automated optimization process by a simple, but representative, boundary condition. Automated generation of the baseplate as well as the parametrization of the rear side of the baseplate is necessary for this.

ACKNOWLEDGMENT

We would like to thank the DLR, Energy Programme Directorate for its support.

REFERENCES

[1] de Pee, A., 2018. "Decarbonization of industrial sectors: the next frontier". *McKinsey and Company*.

[2] Arpagaus, C., 2016. "Multi-temperature heat pumps: A literature review". *International Journal of Refrigeration 69*.

[3] Arpagaus, C., 2018. "High temperature heat pumps: Market overview, state of the art, research status, refrigerants and application potentials". *International Refrigeration and Air Conditioning*.

[4] Arpagaus, C., 2017. "Hochtemperatur wärmepumpen literaturstudie zum stand der technik, der forschung, des anwendungspotenzials und der kältemittel". *Interstaatliche Hochschule für Technik Buchs*.

[5] Duclos, S. D. L. P., 2014. "High temperature gas heat pumps to recover industrial waste heat". *International Gas Union*.

[6] Meroni, A., 2018. "Design of centrifugal compressors for heat pump systems". *Applied Energy 232*.

[7] Wiesner, F. J., 1967. "A review of slip factors for centrifugal impellers". *Journal of Engineering for Power*.

[8] Jin-Hyuk Kim, Afzal Husain, K.-Y. K., 2010. "Multi-objective optimization of a centrifugal impeller through evolutionary algorithms". *Proceedings of the Institution of Mechanical Engineering Part A Journal of Power an Energy*.

[9] Raitor, T., 2013. "Aerodynamic design studies of a transonic centrifugal compressor impeller based on automated 3d-cfd optimization". *10th European Conference on Turbomachinery Fluid dynamics and Thermodynamics*.

[10] Hui Li, D.-G. H., 2017. "Aerodynamic optimization design of a multistage centrifugal steam turbine and its off-design performance analysis". *International Journal of Rotating Machinery Volume 2017, Article ID 4690590*.

[11] Hehn, A., 2018. "Aerodynamic optimization of a transonic centrifugal compressor by using arbitrary blade surfaces". *Journal of Turbomachinery*.

[12] Ratz, J., 2019. "Surge margin optimization of centrifugal

compressors using a new objective function based on local flow parameters". *Turbomachinery Propulsion and Power*.

[13] Cuciumita, C., 2021. "Structurally constrained aerodynamic adjoint optimisation of higly loaded compressor blades". *Proceedings of ASME Turbo Expo 2021*.

[14] Systemtechnologies, S., 13.12.2021. "Universal plant design and optimization". *https://www.steag-systemtechnologies.com/uploads/pics/STEAGFactSheet-EBSILONENNEUANSICHT03.pdf*.

[15] Lachner, B., 2004. "An investigation into the feasibility of the use of water as refrigerant".

[16] Zuehlsdorf, B., 2019. "Analysis of technologies and potentials for heat pump-based process heat supply above 150°c". *Energy Conversaion and Management: X*.

[17] Schmitz, A., 2020. "Multifidelity-optimierungsverfahren für turbomaschinen". *PhD thesis*.

[18] Voss, C., Aulich, M., Kaplan, B., and Nicke, E., 2006. "Automated multiobjective optimisation in axial compressor blade design". *ASME Turbo Expo 2006: Power for Land Sea and Air (GT2006-90420)*.

[19] Goinis, G., and C. Voß, C. u. E. N., 22.-27. Sep. 2019, Canberra, Australien. "The potential of casing treatments for transonic compressors: Evaluation based on axial-slot and rotor blade optimization". *ISABE 2019*.

[20] Schnoes, M., Schmitz, A., Goinis, G., Voß, C., and Nicke, E., 23-27 Sep 2019, Canberra, Australia. "Strategies for multi-fidelity optimization of multi-stage compressors with throughflow and 3d cfd". *ISABE 2019*.

[21] Voß, C., and Nicke, E., 2008. "Automatische optimierung von verdichterstufen". *Technische Informationsbibliothek Hannover*, September.

[22] Sauer, M., 11-15 June 2018, Glasgow, UK. "An optimization based approach to multi-block structured grid generation". *6th European Conference on Computational Mechanics*.

[23] Çengel, Y. A., and Boles, M. A., 2005. "Thermodynamics: An engineering approach". *5th Edition*.

[24] Franke, M., Kügeler, E., and Nürnberger, D., 2005. "Das dlr-verfahren trace: Moderne simulationstechniken für turbomaschinenströmungen". In Deutscher Luft- und Raumfahrtkongress 2005, DGLR, ed.